A new crest height distribution for nonlinear and breaking waves in varying water depths

I. Karmpadakis [*], C. Swan

Department of Civil & Environmental Engineering, Imperial College London, London, SW7 2AZ, UK

A B S T R A C T

The statistical distribution of zero-crossing crest heights represents a critical design input for a wide range of engineering applications. The present paper describes the development and validation of a new crest height model, suitable for application across a broad range of water depths. The purpose of this model is two-fold: first, to describe the amplifications of the largest crest heights arising due to nonlinear interactions beyond a second-order of wave steepness, and second, to incorporate the dissipative effects of wave breaking. Although these two effects act counter to each other, there is substantial evidence to suggest departures from existing models based upon weakly nonlinear second-order theory; the latter corresponding to current design practice. The proposed model has been developed on the basis of a significant collection of experimental results and a small subset of field measurements. It incorporates effects arising at different orders of nonlinearity as well as wave breaking in a compact formulation and covers a wide range of met-ocean conditions. Importantly, the new model has been independently validated against a very extensive database of experimental and field measurements. Taken together, these include effective water depths ranging from shallow water ($k_p d \approx 0.5$) to deep water ($k_p d > 3$) and sea-state steepnesses covering mild, severe and extreme conditions. The new model is shown to provide a significant improvement in crest height predictions over existing methods. This is particularly evident in the steepest, most severe sea-states which inevitably form the basis of design calculations.

1. Introduction

The distribution of crests heights arising within specific sea-states or storms is a key input for the design and re-assessment of most marine structures. For example, one crucial aspect in the design of many new structures concerns the avoidance of wave-in-deck (WID) loading. Likewise, accurate loading calculations are essential for the re-assessment of existing structures. A first step in addressing these issues is to assess whether WID loading actually occurs. The key to answering this lies in the height of the largest crests relative to the underside of the deck structure. In other words, the occurrence of such loads is determined by the distribution of crest heights; particularly the largest crests in the most severe ("design") conditions. Moreover, the magnitude of the WID load is, in large part, determined by the crest heights; the former being critically dependent upon the level of deck inundation (Ma and Swan, 2020). As such, the importance of crest height predictions lies in both the potential occurrence of WID loading and the magnitude of the loading that results.

Traditional oil & gas applications, the rapidly expanding offshore wind energy sector, and different types of marine renewable devices are all examples for which accurate crest height calculations are essential. Importantly, such applications occur in a wide variety of deep, intermediate and shallow water depths. As such, successful crest height predictions must be achievable across the full range of effective water depths.

In this context, the success of a crest height distribution is defined by its potential to incorporate both the amplifications associated with fully nonlinear wave–wave interactions and the dissipative effects of wave breaking. Evidence of the importance of these effects is given in Latheef and Swan (2013) and Karmpadakis et al. (2019); the former relating to deep water and the latter intermediate water depths. Whilst the findings in these studies were largely based upon laboratory data, Fig. 1 provides characteristic examples based upon water surface elevations recorded in the field. In both subplots, the exceedance probability (Q) of the normalised crest heights (η_c/H_s) is compared to the most widely applied models in engineering design. These models include effects arising either at the first (linear) or second-order of wave steepness (Forristall, 2000); the latter representing the recommended practice in most design codes (DNV-RP-C205, ISO 19901-1). Fig. 1(a) shows data recorded at a deep water location ($d = 110\,\text{m}$), in which the
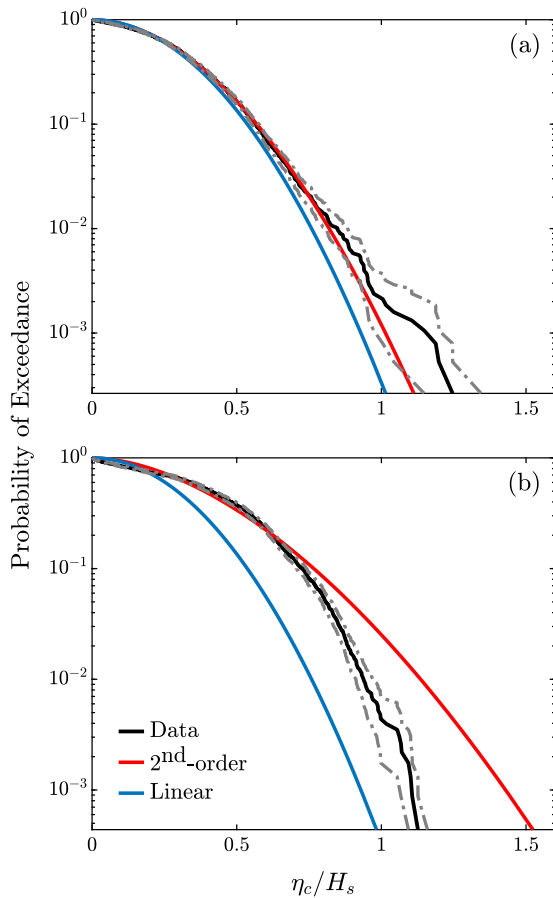

Fig. 1. Examples of normalised crest height distributions, η_c/H_s, recorded in the field and showing comparisons to linear and second-order predictions. The data relate to: (a) $H_s = 8$ m, $T_p = 10$ s, $d = 110$ m and (b) $H_s = 4.5$ m, $T_p = 9.5$ s, $d = 7.7$ m. The 95% credible intervals have been added for reference.

largest crest heights are notably larger than the design (second-order) predictions. In this case, design predictions appear to align with the lower bound of the 95% confidence intervals of the data. In contrast, Fig. 1(b) shows measurements at a shallow water location ($d = 7.7$ m). In this case the largest measured crest heights lie between the linear and second-order predictions; both models clearly misrepresenting the measured field data.

Taken together, the two examples on Fig. 1 are representative of a wide range of environmental conditions and illustrate the motivation behind the present study: that measured crest heights in severe sea-states can be either under-predicted or over-predicted by present design solutions. To address this issue, a new crest height model is developed. This is capable of describing the short-term distribution of crest heights in a wide range of sea-state steepnesses and water depths; the latter covering deep, intermediate and shallow water conditions. The new model captures higher-order nonlinear effects as well as wave break-ing, and has been calibrated using a large database of experimental measurements. Importantly, the proposed model is validated against both experimental and field measurements and is shown to provide an improved description of the measured crests heights in all water depths. This is important for two reasons. First, it provides a model that can be seamlessly integrated into the design process; removing the requirement to use different models for different conditions or loca-tions. Second, it shows that the parametrisation of the model captures the main physical processes defining the crest heights in a wide range of water depths.

The contents of this paper are arranged as follows. First, a brief overview of literature relevant to the distribution of crest heights is given in Section 2. The characteristics of the experimental and field measurements are then presented in Section 3. Section 4 provides fundamental insights into crest height distributions and presents the development of a new crest height model. The validation of the new model is discussed in Section 5, with key conclusions arising from the study provided in Section 6.

2. Background

Having noted the practical importance of crest height predictions, it is not surprising that several studies have addressed their short–term distribution. Among these, the Rayleigh (Longuet-Higgins, 1952; Tayfun, 1980; Forristall, 2000; Tayfun and Fedele, 2007) distributions are the most widely applied. These models cover effects arising at increasing orders of nonlinearity; the latter being expressed in terms of effective wave steepness (αk), where α represents the wave amplitude and k the wavenumber. Taken together, these models cover the first three orders of wave steepness and have been extensively validated and assessed using a wide range of wave conditions (Latheef and Swan, 2013; Karmpadakis et al., 2019).

The key characteristics of the aforementioned models are sum-marised below:

(a) Rayleigh distribution (Longuet-Higgins, 1952)

This is the first-order (linear) model that describes crest heights arising in a Gaussian sea-state. Its functional form is defined as:

$$Q(\eta_c) = \exp\left[-8\left(\frac{\eta_c}{H_s}\right)^2\right],\tag{1}$$

where Q is the exceedance probability, η_c the crest heights and H_s the significant wave height. The significant wave height is calculated using its spectral definition as

$$H_s = 4\sqrt{m_0} = 4\sigma_\eta,\tag{2}$$

where σ_η is the standard deviation of $\eta(t)$ and m_0 is the zeroth spectral moment. Using the variance spectrum, $S_{\eta\eta}(f)$, the spectral moments of order n are described by:

$$m_n = \int_0^\infty f^n S_{\eta\eta}(f)\mathrm{d}f,\tag{3}$$

where f represents the frequency of individual wave harmonics. Bound by the assumption of linearity, the Rayleigh distribution is known to significantly under-estimate the largest crests, or those arising at small exceedance probabilities.

(b) Tayfun distribution (Tayfun, 1980)

Considering nonlinear effects arising at a second-order of wave steepness and a narrowband approximation, Tayfun (1980) derived an analytical model to describe the crest height distribution. This is given by:

$$Q = \exp\left[-\frac{\left(-1 + \sqrt{1 + 8\mu\frac{\eta_c}{H_s}}\right)^2}{2\mu^2}\right],\tag{4}$$

where μ is a measure of wave steepness that accounts for second-order nonlinearities. In its original form, μ was related to the sea-state skewness, λ_3, through:

$$\mu = \frac{\lambda_3}{3} \quad \text{and} \quad \lambda_3 = \frac{\langle(\eta - \bar\eta)^3\rangle}{m_0^{3/2}};\tag{5}$$

the angled brackets denoting a statistical average. Despite the assumed narrow-bandedness, this model has been broadly validated using real-istic sea-state conditions (Fedele et al., 2016, 2019). This involves the employment of improved definitions for μ provided by Tayfun (2006) and Fedele and Tayfun (2009).

(c) Forristall (3D) distribution (Forristall, 2000)

This model is the most widely applied in engineering practice. It has been derived as a fit to numerical simulations of second-order random wave theory (Sharma and Dean, 1981). Its functional form is a two-parameter Weibull distribution, defined as:

$$Q = \exp\left[-\left(\frac{\eta_c}{\alpha H_s}\right)^{\beta}\right], \tag{6}$$

where the scale, α, and shape, β, parameters for short-crested sea-states are given by:

$$\alpha = 0.3536 + 0.2568\,S_1 + 0.0800\,Ur \tag{7}$$
$$\beta = 2 - 1.7912\,S_1 - 0.5302\,Ur + 0.2824\,Ur^2.$$

In defining these coefficients, the mean sea-state steepness, S_1, and Ursell number, Ur, are calculated by:

$$S_1 = \frac{2\pi H_s}{g T_1^2} \quad \text{and} \quad Ur = \frac{H_s}{k_1^2 d^3}. \tag{8}$$

The mean wave period, $T_1 = m_0/m_1$, is obtained using Eq. (3), k_1 is the wavenumber corresponding to T_1 based upon the linear dispersion relation and d is the water depth. The coefficients in Eq. (7) relate to the short-crested version of the model; the corresponding coefficients for long-crested seas can be found in Forristall (2000).

(d) Tayfun & Fedele distribution (Tayfun and Fedele, 2007)

This is a third-order model derived on the basis of a Gram–Charlier series expansion. This method of representation has previously been applied in the description of water surface elevations and related wave statistics by Longuet-Higgins (1963) and Bitner (1980), as well as wave envelopes and phasing by Tayfun and Lo (1990), Tayfun (1994). The functional form of the model is given by:

$$Q = \exp\left[-\frac{\left(-1 + \sqrt{1 + 8\mu\frac{\eta_c}{H_s}}\right)^2}{2\mu^2}\right]\left\{1 + \Lambda\left(\frac{\eta_c}{H_s}\right)^2\left[4\left(\frac{\eta_c}{H_s}\right)^2 - 1\right]\right\}, \tag{9}$$

where μ is defined in Eq. (5) and Λ is a parameter that captures third-order nonlinearities. It is defined on the basis of fourth-order cumulants of the surface elevation, η, and its Hilbert transform, $\hat{\eta}$, as:

$$\Lambda = \lambda_{40} + 2\lambda_{22} + \lambda_{04}, \quad \text{and} \tag{10}$$
$$\lambda_{mn} = \frac{\langle \eta^m \hat{\eta}^n \rangle}{\sigma_\eta^{m+n}} + (-1)^{m/2}(m-1)(n-1) \tag{11}$$

The predictions of these models are compared to laboratory measurements of short-crested sea-states obtained at Imperial College London in Fig. 2. Specifically, Fig. 2(a) concerns a nonlinear sea-state with steepness $S_1 \approx 0.04$ in intermediate water $k_1 d \approx 2$. This sea-state is characterised by very limited or no wave breaking. Based upon the comparisons provided, it is clear that the Rayleigh distribution significantly underestimates the measured crest heights. The inclusion of second-order nonlinearities within the Tayfun and Forristall models provides an improvement, although the largest measured crest heights remain under-predicted. However, the incorporation of third-order nonlinearities through the Tayfun & Fedele model results in good agreement with the laboratory data. In contrast, Fig. 2(b) concerns a must steeper sea-state ($S_1 = 0.07$). This is characterised by significant wave breaking in the same effective water depth. In this case, the tail of the measured crest height distribution has reduced due to wave breaking and lies immediately below the predictions of the second-order models. Wave breaking has also led to a notable increase in smaller crest heights lying at probabilities $Q \approx 10^{-1}$. As discussed in Karmpadakis et al. (2019), the occurrence of substantial wave breaking will reduce the H_s of the sea-state relative to what it would have been had no wave breaking occurred. While the largest and steepest waves are more likely to undergo some form of energy dissipation, there will remain a large number of less steep waves that will not
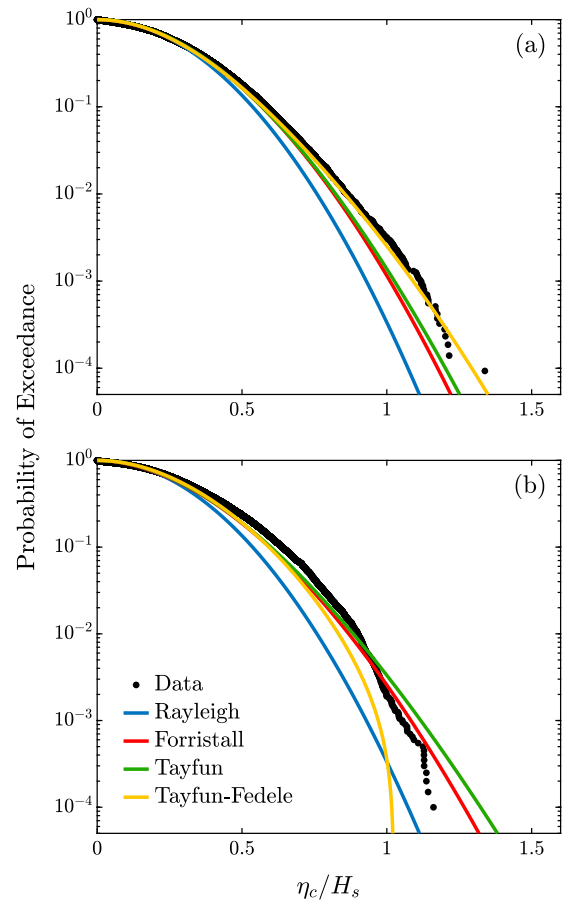

Fig. 2. Comparisons of existing crest height models using short-crested experimental data for: (a) a steep but non-breaking sea-state ($S_1 \approx 0.04$, $k_1 d \approx 2$), and (b) a very steep sea-state with significant wave breaking ($S_1 \approx 0.07$, $k_1 d \approx 2$).

break. Since these waves will be normalised by a reduced H_s, they will "appear" to be amplified beyond the second-order distribution. As such, the observed increases in crest heights for $Q \approx 10^{-1}$ are primarily associated with wave breaking and the commonly applied normalisation, rather than non-linear amplification. In addition to the changes in H_s, wave breaking also influences higher-order integral parameters of the sea-state. This directly effects the third-order nonlinearity parameter Λ [Eq. (10)], leading to the divergence of the Tayfun & Fedele model.

As indicated in Fig. 2, the two second-order distributions are closely aligned. The inclusion of second-order effects is frequently considered sufficient to describe crest height statistics (e.g. Fedele et al., 2019). However, both Figs. 1 and 2 suggest that higher order effects and wave breaking play an important role in both experimental and field measurements. This is also supported by increasing evidence in other field (Andreasen et al., 1997; Bitner-Gregersen and Magnusson, 2004; Petrova et al., 2006; Gibson et al., 2014), experimental (Cherneva et al., 2009; Onorato et al., 2009; Buchner et al., 2011; Latheef and Swan, 2013) and numerical studies (Socquet-Juglard et al., 2005; Xiao et al., 2013; Zve, 2022).

While the majority of these studies relate to deep water, recent results by Karmpadakis et al. (2019) and Schubert et al. (2020) have indicated that these effects retain their importance within intermediate and shallow water. As such, the present work seeks to describe their behaviour across the full range of water depths.

3. Available data and methods

The development and validation of a new crest height distribution has been based upon two different sources of data: laboratory simulations and field measurements. The key characteristics of each are discussed below.

3.1. Laboratory data

The data employed in the present work come from 4 different experimental campaigns. Three of these campaigns (Tests A–C) were conducted at Imperial College London (ICL), while the fourth dataset (Test D) was generated independently at the Danish Hydraulics Institute (DHI). Taken together, the experimental data cover effective water depths lying in the range $0.85 \leq k_p d \leq 3.5$ and a very wide range of sea-state conditions; the latter defined by steepness (S_p) and directional spread (σ_θ). Importantly, the available data were subdivided in two non-overlapping datasets; the first (Tests A–B) used for the derivation of the model and the second (Tests C–D) for its validation.

The deep-water wave basin at ICL was used for the generation of Tests A–C. This consists of 56 individually controlled wave paddles, operating with force-feedback control. The combination of a passively absorbing beach and active wave absorption at the paddles leads to high quality wave measurements with particularly good accuracy in the directional characteristics. The facility has been extensively validated in a series of previous studies including Masterton and Swan (2008), Spinneken and Swan (2012), Latheef et al. (2017) and Karmpadakis et al. (2019).

Each generated sea-state is defined using 3 variables:

(i) the significant wave height, H_s,
(ii) the spectral peak period, T_p, and
(iii) the directional spreading parameter, σ_θ.

In these cases, σ_θ, corresponds to the standard deviation of a wrapped normal directional spreading function, $D(\theta)$, given by:

$$D(\theta) = \frac{A}{\sigma_\theta} \exp\left(\frac{-\theta^2}{2\sigma_\theta^2}\right), \tag{12}$$

where A is a normalising parameter and θ represents the propagation angles of individual wave harmonics relative to the mean wave direction; the latter always defined perpendicular to the paddle face.

All the tests presented in this study correspond to short-crested sea-states based upon the standard JONSWAP frequency spectrum defined by Hasselmann et al. (1973) as:

$$S_{\eta\eta}(f) = \frac{\alpha g^2}{(2\pi)^4 f^5} \exp\left[-\frac{5}{4}\left(\frac{f}{f_p}\right)^{-4}\right]\gamma^{G(f)}, \tag{13}$$

$$\text{where } G(f) = \exp\left[-\frac{1}{2}\left(\frac{f/f_p - 1}{\sigma}\right)^2\right] \tag{14}$$

is the peak enhancement function with $\gamma = 2.5$ (Holthuijsen, 2007), α the energy scale factor, f_p the spectral peak frequency and $g = 9.81 \, \text{m s}^{-2}$ the gravitational acceleration. The peak width parameter was defined as $\sigma = 0.07$ for $f \leq f_p$ and $\sigma = 0.09$ for $f > f_p$. The two-dimensional wave spectrum, $E(f,\theta)$, is then given by:

$$E(f,\theta) = S_{\eta\eta}(f)D(\theta), \tag{15}$$

Using Eq. (12)–Eq. (15), 20 random simulations (or seeds) were generated for each sea-state. Each simulation had a duration of approximately 3 h (at full-scale) and was recorded using state-of-the-art wave gauges with a high sampling rate ($f_s = 128 \, \text{Hz}$). Since all the simulations correspond to the same underlying spectrum, they can be treated as random realisations of the same storm. In combining all the seeds for a given sea-state and applying a zero-crossing analysis, the representative crest heights for that sea-state can be extracted. The total

Table 1
Test A: sea-state characteristics for test cases conducted in the ICL wave basin with $d = 125 \, \text{m}$.

Case	H_s [m]	T_p [s]	$k_p d$	σ_θ [°]
AA1	8.7	12	3.5	15
AA2	15			15
AB1	11.7	14	2.6	15
AB2	15			15
AC1	3			15
AC2	10			15, 30
AC3	12.5	16	2.03	15
AC4	15			15, 30
AC5	17.5			15
AC6	20			30

Table 2
Test B: sea-state characteristics for test cases conducted in the ICL wave basin with $d = 50 \, \text{m}$.

Case	H_s [m]	T_p [s]	$k_p d$	σ_θ [°]
BA1	2.2			
BA2	4.4			
BA3	6.7			
BA4	8.9	12	1.53	10, 20
BA5	11.2			
BA6	13.4			
BA7	15.7			
BB1	3			
BB2	6.1			
BB3	9.1	14	1.22	10, 20
BB4	12.2			
BB5	15.3			
BB6	18.3			
BC1	4			
BC2	8			
BC3	9.1	16	1.02	10, 20
BC4	12			
BC5	16			

number of crest heights per sea-state varies with T_p; typically lying between 15,000–20,000. This is sufficiently high to describe the largest waves or those arising at very low probabilities of exceedance. The method described above has been routinely applied in the analysis of experimental measurements; a more detailed description being given in Karmpadakis et al. (2019).

The characteristics of Tests A–C are provided in Tables 1–3. This data is presented as equivalent full-scale values based on an adopted length-scale of $L_s = 1/100$ and a corresponding time-scale of $t_s = \sqrt{L_s} = 1/10$. In general, Test A concerns sea-states representative of "design" conditions in relatively deep water ($d = 125 \, \text{m}$) with directional spreading varying between 15° and 30°; more details being provided in Latheef and Swan (2013). Test B concerns sea-states in intermediate water depths ($d = 50 \, \text{m}$) with increasing deep-water steepness varying from near-linear, $S_p = 0.01$, to highly nonlinear, $S_p = 0.07$. The directional spreading in Test B varies between 10° and 20°, while full details can be obtained in Karmpadakis et al. (2019), Karmpadakis and Swan (2020). Test C, again, concerns "design" sea-states in a range of water depths, $d = 125 \, \text{m}$, 90 m and 50 m, and directional spreading $\sigma_\theta = 10°$ and 20°.

The experimental measurements in Test D were conducted in a water depth of 45 m in the DHI wave basin. The focus of these test cases has also been to investigate steep sea-states in intermediate water depths; the details of which are given in Table 4. This data is also presented as equivalent full-scale values, the adopted scaling being $L_s = 1/90$ and $t_s = 1/9.5$. Within this dataset, the peak enhancement factor, γ, in Eq. (13) varied between 1–5. In addition, the directional spreading function was frequency-dependent, based on the cosine2s distribution function outlined in Mitsuyasu et al. (1975). For consistency, in the presentation of results that follows, these test cases

Table 3
Test C: sea-state characteristics for test cases conducted in the ICL wave basin with variable water depth.

Case	H_s [m]	T_p [s]	$k_p d$	σ_θ [°]	d [m]
C1	15	14	2.6	20	
C2	15	16	3.5	10, 20	125
C3	17.5	16	3.5	20	
C4	15	14	1.93	20	
C5	15	16	1.55	20	90
C6	17.5	16	1.55	20	
C7	15	14	1.22	20	
C8	15	16	1.02	10, 20	50
C9	17.5	16	1.02	20	

Table 4
Test D: sea-state characteristics for test cases conducted in the DHI wave basin with $d = 45$ m.

Case	H_s [m]	T_p [s]	$k_p d$	σ_θ [°]
DA1	11	10.5	1.75	17.7, 33.1
DB1	8.4	12.5		33.1
DB2	10	12.5	1.33	17.7, 33.1
DB3	11	12.5		17.7, 33.1
DB4	12	12.5		10, 17.7, 33.1
DC1	8.4	15		33.1
DC2	10	15		17.7, 33.1
DC3	11	15	1.03	10, 17.7, 33.1
DC4	12	15		10, 17.7, 33.1
DC5	13	15		10, 17.7, 33.1
DD1	10	17.5		17.7
DD2	11	17.5	0.85	10, 17.7, 33.1
DD3	12	17.5		10, 17.7, 33.1
DD4	13	17.5		10, 33.1

will be described using the corresponding wrapped normal directional spreading [Eq. (12)], which varied between $\sigma_\theta = 10°$, 17.7° and 33.1°.

3.2. Field data

In addition to the experimental data, a large database of field measurements has been analysed to provide further insights into the distribution of crest heights and to validate the proposed model. These have been obtained using wave radars mounted on the side of fixed offshore North Sea platforms, the corresponding water depths lying between 7.7 m and 189 m. The locations of the 21 platforms considered are shown on Fig. 3, with details of the water depths and number of available sea-states given in Table 5.

The key steps in the analysis of raw field records are summarised as follows. First, the measured "air-gap" was inverted to produce the required water surface elevation records, $\eta(t)$, with any tidal or surge components removed. The resulting zero-mean records were divided into individual sea-states of 20-minute duration. Each sea-state was quality controlled (QC'd) using the methodology proposed by Christou and Ewans (2014) and modified by Karmpadakis et al. (2020). This procedure identifies erroneous measurements through a series of flags and discards them from the dataset. The QC'd sea-states were, subsequently, analysed using standard time–frequency techniques to obtain met-ocean parameters (such as H_s and T_p), zero-crossing crest heights (η_c) and other spectral parameters.

The QC'd data arising in each measuring station were then subject to stratified sampling to yield the final dataset under consideration. In this respect, the data relating to individual sea-states are grouped (or binned) to yield larger datasets with similar characteristics. This was achieved by selecting small increments of representative met-ocean parameters, such as H_s, T_p and S_1. Within this study, the size of each bin was defined in the (H_s, T_p) parameter space and had widths of $\Delta H_s = 0.5$ m and $\Delta T_p = 0.5$ s. As part of this grouping, each data bin is taken to represent a sea-state with characteristics that correspond
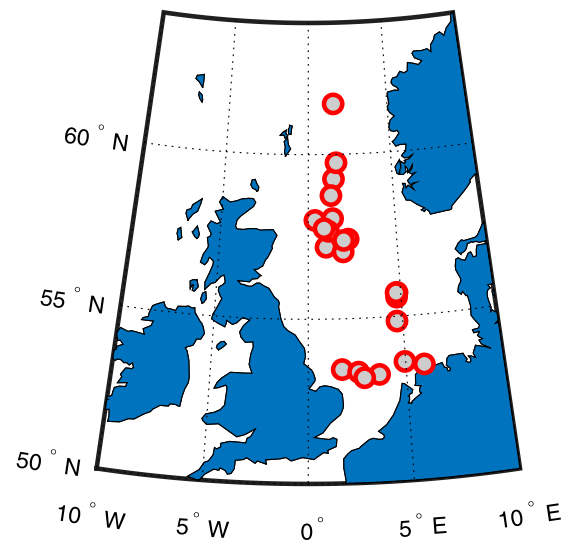

Fig. 3. Map of measuring locations in the North Sea.

to the mean of all the sea-states that define it. In other words, key met-ocean parameters are calculated from the sea-states in all bins separately and are then averaged to represent each bin. One important use of these parameters lies in the definition of the theoretical crest height distributions; for example, the S_1 and Ur parameters that are required as input in the Forristall (2000) model [Eq. (7)]. Additionally, the zero-crossing crest heights arising within each sea-state in a data bin are normalised by their corresponding significant wave height, H_s, and concatenated to provide empirical crest height distributions representative of their data bin.

Alongside an efficient quality control procedure for the raw field measurements, it is worth noting that the nature of the data is well suited to investigate crest height statistics. This is because they have been recorded using fixed instruments and high sampling rates, $f_s \geq 4$ Hz. Alternative measuring techniques, such as wave buoys, are known to underestimate crest heights either due to their hydrodynamic properties (Allender et al., 1989; Rademakers, 1993; James, 1986; Magnusson et al., 1999) or low sampling frequency (Tayfun, 1993; Stansell et al., 2002). This underestimation might be less relevant in smaller sea-states (Casas-Prat and Holthuijsen, 2010) and could potentially be partially resolved using approximations (Herbers and Janssen, 2016; McAllister and van den Bremer, 2019). However, any underestimation in the largest crest heights could be very misleading in the context of engineering design. As such, the analysis of measurements that can accurately capture the largest crest heights is of significant value.

Subsets of this database have been previously presented in the context of wave height distributions (Karmpadakis et al., 2020). However, this is the first time that data relating to crest heights have been combined to cover such a wide range in water depths. Taken together, the final (QC'd) dataset contains approximately 2 million sea-states (Table 5) which makes it one of the largest datasets of this type in the literature.

Given the nature of the analysis to follow, it is very important that good agreement is observed between the field and laboratory data when similar conditions are considered. Evidence of this agreement is shown through the crest and wave height distributions on Fig. 4 alongside comparisons to the Rayleigh and Forristall models. The data that are being compared have the same met–ocean parameters ($S_p = 0.03$ and $k_p d \approx 1.2$) and show close agreement in both crest and wave heights. This confirms that the experimental procedure can generate data that are entirely representative of the measured field conditions. Similar findings have been reported by Karmpadakis (2018) across a wide range of test cases. This is particularly important considering the

Table 5
Sources of field data indicating platform names, water depths with respect to mean sea water level and number of 20-min sea-states.

ID	Platform name	Water depth [m]	No. sea–states
P1	Magnus	189	70,937
P2	Unity	123	77,309
P3	Bruce	121	80,499
P4	Goldeneye	121	111,719
P5	Andrew	117	77,429
P6	Harding	110	57,816
P7	Miller	100	72,769
P8	ETAP	94	77,426
P9	Gannet	94	103,894
P10	Mungo	91	77,121
P11	Shearwater	89.3	106,172
P12	Nelson	84.5	87,845
P13	Gorm	40	6,081
P14	F03	42.35	14,151
P15	TyraW	45	7,667
P16	Leman	35.76	192,010
P17	Sean	32.26	132,087
P18	K14	27.36	147,743
P19	L9	24.98	107,488
P20	Clipper	23.3	198,323
P21	AWG	7.7	110,896

Fig. 5. Bar plots indicating the ratio between measured crest heights and the predictions of the Forristall (3D) distribution, η_c/η_F, arising at a probability level of $Q = 10^{-3}$. The data correspond to a range of sea-state steepnesses, S_p, for 3 effective water depths: (a) $k_p d = 2.03$, (b) $k_p d = 1.53$ and (c) $k_p d = 1.02$ and directional spreads of (a) $\sigma_\theta = 15°$ and (b, c) $\sigma_\theta = 10°$. Error bars (black lines) indicating the 95% confidence intervals have been added for reference.

Fig. 4. Normalised crest height, η_c/H_s, and wave height distributions, H/H_s, recorded in the laboratory (BA3) and the field (P13) for similar met–ocean conditions ($S_p = 0.03$ and $k_p d \approx 1.2$). The Rayleigh and Forristall crest height and wave height distributions have been added for reference.

potential differences between the laboratory and the field; examples of the latter include different wave generation mechanisms, spectral evolution over large distances and subsequent nonlinear changes, and the presence of winds or currents. Despite the observed agreement, the difference in the amount of data between field ($\approx 2{,}500$ waves) and experimental measurements ($\approx 22{,}000$ waves) is clear. This emphasises the importance of long experimental simulations that can produce results with very low exceedance probabilities. This is not possible with field measurements in which the data records are considerably shorter, particularly for the most extreme storms. This, in turn, justifies the approach of using experimental data for the calibration of the proposed model, and field measurements to provide an independent validation.

4. Model development

4.1. Physical insights

It has already been established that the Forristall and Tayfun crest height models can adequately capture effects arising at a second-order of wave steepness. In addition, the results presented in Figs. 1 and 2 have clearly indicated the competing mechanisms of nonlinear amplification and wave breaking in the formation of the largest crest heights.
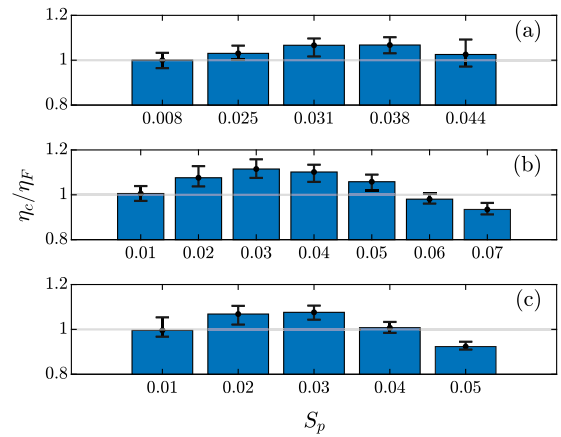
As such, it is worth identifying the extent of nonlinear interactions above second-order and the dissipative effects of wave breaking across a wide range of wave conditions.

To achieve this, the measured data are normalised with respect to second-order predictions. Specifically, the ratio of measured crest heights (η_c) over the corresponding predictions of the Forristall model (η_F) are investigated. The latter are obtained from an inversion of the Forristall probability model:

$$\eta_F = \alpha H_s \left(-\ln Q\right)^{1/\beta}, \tag{16}$$

where the distribution parameters α and β for the short-crested version of the model are provided in Eq. (7). Having shown that the predictions of the Forristall and Tayfun models are in close agreement (Tayfun, 2006), only the former is used in the present analysis due to its wider inclusion in design calculations. However, similar results would arise if the Tayfun model was used instead.

In Fig. 5, bar plots are used to represent the ratio of experimentally recorded crest heights over the corresponding second-order predictions (η_c/η_F) for an exceedance probability of $Q = 10^{-3}$. This has been selected as representative of the largest crest height arising in a 3-hour sea-state with a mean zero-crossing period $T_z = 10$ s. In determining the corresponding crest heights from the experimental records, all 20 simulations of each sea-state within cases AC, BA and BC have been considered. These are characterised by effective water depths $k_p d = 2.03, 1.53$ and 1.02, as well as directional spreads of (a) $\sigma_\theta = 15°$ and (b,c) $\sigma_\theta = 10°$. Within each subplot, the results are ordered with increasing sea-state steepness in the horizontal axis. Finally, 95% confidence intervals have been calculated using 10,000 bootstrap samples and superimposed on each case.

There are two key conclusions arising from the results presented on Fig. 5. First, the examination of each subplot in isolation (constant $k_p d$) suggests that increasing sea-state steepness, S_p, leads to statistically significant deviations from the second-order model. While the crest heights arising in the lowest steepness cases are well described by second-order predictions, amplifications of up to 10% develop for $S_p \approx 0.03 - 0.04$. These are introduced by nonlinear interactions above second-order and are shown to be outside the expected statistical variability indicated by the confidence intervals. Further increases in sea-state steepness reverse this effect and lead to progressively lower η_c/η_F. Reductions of the order of 8% with respect to second-order predictions arise for the steepest cases. These can be clearly identified in the BA ($k_p d = 1.53$) and BC ($k_p d = 1.02$) test cases, in which a
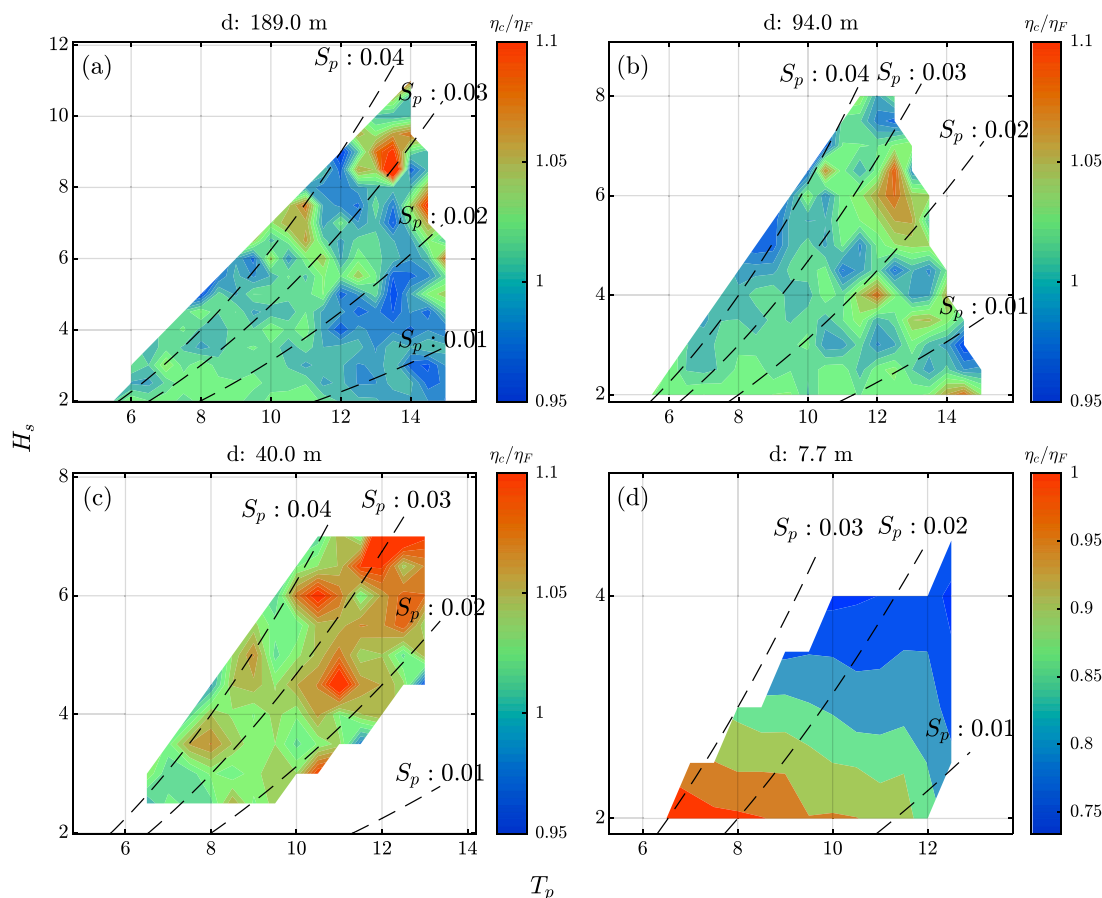
Fig. 6. Contour maps indicating the ratio of measured crest heights over second-order predictions (η_c/η_F) for exceedance probabilities $Q = 10^{-3}$. The results are obtained using stratified sampling on the $H_s - T_p$ parameter space and correspond to platforms: (a) P1, (b) P9, (c) P13 and (d) P21. Lines of constant sea-state steepness (S_p) have been added for reference.

wider range of incident conditions has been examined. The explanation of these reductions lies in the energy dissipation due to wave breaking. In this respect, both spilling and overturning wave breaking was extensively observed in the experimental simulations of these steep sea-states. The second observation relates to the relevance of these trends across different effective water depths. Indeed, it can be seen that they remain important over the full range of water depths investigated in this study; from deep water to the shallow end of the intermediate water depth regime. Interpreting these results in conjunction with the earlier findings of Latheef and Swan (2013) and Karmpadakis et al. (2019), it can be concluded that the incorporation of both higher–order nonlinear effects and wave breaking is key to the development of a crest height model applicable to all water depths.

The departure of crest heights measured in the field from second-order predictions can be investigated using a similar methodology. In this case, the stratified sampling ("data binning") approach described in Section 3.2 is employed. Upon discretising the $H_s - T_p$ parameter space, the crest height ratio η_c/η_F arising for exceedance probabilities of $Q = 10^{-3}$ is calculated for each data bin. Fig. 6 presents the results arising in 4 selected locations in the form of contour plots. These locations have been selected to cover the widest range of water depths, which vary between 189 m and 7.7 m. As such, the data include incident wave conditions in deep, intermediate and shallow water depth conditions.

The contour map on Fig. 6(a) shows the data arising in the deepest field location ($d = 189$ m). It can be seen that the majority of the sea-states demonstrate small deviations from the Forristall predictions. This is particularly apparent in the bottom half of the contour plot ($H_s < 6$ m), where the deviations are typically ±3%. However, larger deviations from the second-order predictions are observed in the top

half of the contour plot, which contains more severe sea-states ($H_s > 6$ m). In some sea-states the measured crest heights are shown to be 10% larger than the corresponding second-order values. In superimposing lines of constant sea-state steepness, S_p, it can be seen that the largest amplifications arise for severe sea-states with $S_p \approx 0.03$. This observation is in agreement with the laboratory findings presented in Fig. 5(a).

Similar results are obtained when considering the measurements in Figs. 6(b) and 6(c) for water depths 94 m and 40 m, respectively. It is worth noting that the data presented in subplot (c) correspond to segmental recordings during severe weather conditions rather than continuous measurements throughout the years. This justifies the lack of sufficient data for low H_s values. More importantly, the magnitude of the discrepancies agrees well with the experimental observations of Fig. 5 in the intermediate water depth regime. It is also worth noting that significant nonlinearities are associated with the formation of large waves in steep sea-states even in cases which show agreement with the second-order model (Katsardi and Swan, 2011). As discussed by Katsardi et al. (2013) the dissipation induced by wave breaking acts to reduce the nonlinear amplifications towards the second-order predictions, particularly in shallower water depths.

In considering the data presented on Fig. 6(d), relating to the shallowest location ($d = 7.7$ m), a different situation clearly arises. In this case, the majority of the measurements fall below the second-order predictions. Indeed, only the mildest sea-states (at the bottom of the contour) are well described by the theory. In the most severe sea-states reductions of the order of 25% can be observed. These effects are a direct consequence of extensive wave breaking and the associated energy dissipation. The magnitude of the discrepancies clearly indicates the need to incorporate wave breaking in the prediction of crest heights.
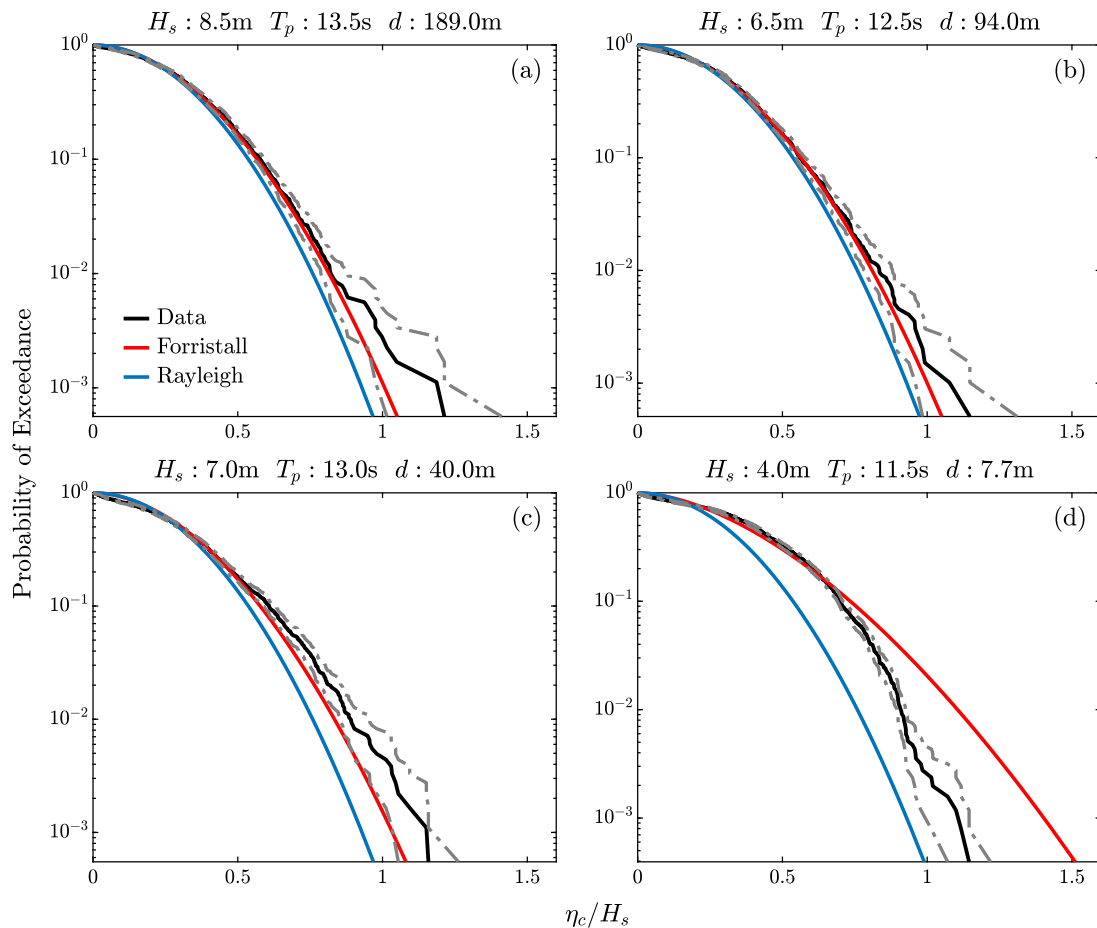
Fig. 7. Normalised crest height distributions, η_c/H_s, recorded in the field with comparisons to linear (Rayleigh) and second-order (Forristall) predictions. The subplots represent selected data bins within locations: (a) P1, (b) P9, (c) P13 and (d) P21, in accordance with the contour plots of Fig. 6. Depth and sea-state information are included in the subplot titles.

The data presented in Fig. 6 provide a thorough representation of discrepancies with respect to second-order predictions across a wide range of incident conditions. It is shown that the large amplifications recorded in the experiment are also present in field measurements at more than one location. This observation arises despite the inherent limitations induced by the reduced data availability in the field. More-over, the importance of wave breaking in reducing large crest heights is clearly established. This is particularly apparent in the shallower locations with depth-limited wave breaking. However, the contours presented in Fig. 6 are restricted to crest heights arising at a single quantile ($Q = 10^{-3}$). To verify the importance of the observed trends, complete crest height distributions are required. Fig. 7 provides the ex-ceedance probabilities of selected sea-states arising in each of the four locations considered previously and extend the field observations pre-sented in Fig. 1. Specifically, normalised crest heights, η_c/H_s, recorded in the field are plotted against the linear (Rayleigh) and second-order (Forristall) predictions, together with their 95% confidence intervals.

The crest height distribution at the deepest location is considered in Fig. 7(a). This corresponds to $k_p d = 4.18$ and $S_p = 0.03$. It can be seen that the measured crest heights consistently diverge from the Forristall model for exceedance probabilities $Q < 10^{-2}$. At the same time, the lower confidence bounds approximate the second-order predictions. This result verifies that the amplifications identified in Fig. 6 for $Q = 10^{-3}$ extend to a wider range of probabilities. The relatively large width of the confidence intervals also reflects the inherent difficulty in using field data for this type of analysis. The finite amount of available data during severe weather conditions, even for large datasets, intro-duces significant statistical variability. As such, examination of these

results in conjunction with experimental measurements, such as those presented earlier, is necessary for an accurate interpretation. In this respect, laboratory measurements in the Test A series (Table 1) with similar sea-state conditions agree well with the present results.

A similar situation arises when data in the intermediate water depth regime are considered in Figs. 7(b) and 7(c). These relate to a sea-state steepness of $Sp = 0.027$ and effective water depths of $k_p d = 2.46$ and $k_p d = 1.16$, respectively. Once again, these results are in agreement with the experimental findings presented earlier and extend the analysis of a single quantile. Lastly, the results arising in the shallowest location in Fig. 7(d) show the extent of differences between measured and predicted values. In this case, the effective water depth is $k_p d = 0.48$ and the sea-state steepness $S_p = 0.017$. The measured crest heights lie approximately mid-way between linear and second-order predictions and are not well described by either model. At the same time, the tail of the distribution is characterised by a much sharper drop-off when compared to either the linear or second-order models. This confirms the occurrence of extensive wave breaking; the energy dissipation producing the characteristic shape in the crest height distribution (Karmpadakis et al., 2019, 2020).

Having established the relevance of a single quantile to describe the departures of the large crest heights from second-order predictions, this representation is employed to provide a general overview of all the available field data. In this respect, Fig. 8 shows the crest height ratio, η_c/η_F, for $Q = 10^{-3}$ across all measuring locations. This is achieved using a swarm chart in which the y-axis corresponds to η_c/η_F and the x-axis to individual measuring locations ordered in descending water depth. Each point in the chart represents a data bin in the
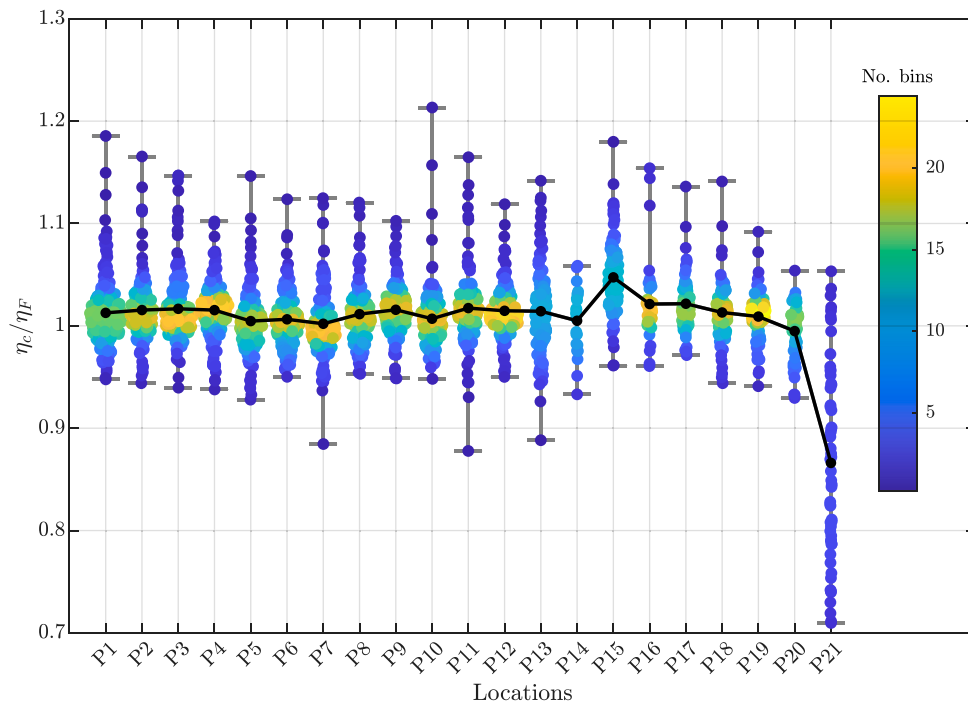
Fig. 8. Swarm chart indicating the ratio of measured crest heights to second-order predictions, η_c/η_F, for exceedance probabilities of $Q = 10^{-3}$ across all available measuring locations. Each point represents the ratio arising in a single data bin. The colormap indicates the number of data bins with a given ratio at each location. The black dotted line shows the mean crest height ratio corresponding to all data bins at each location. (For interpretation of the references to colour in this figure legend, the reader is referred to the web version of this article.)

$H_s - T_p$ parameter space, as defined in Section 3. The density of η_c/η_F within each location is used to colour and offset the data points in the horizontal axis. The mean crest height ratio arising at each location is indicated using a black dotted line.

The data presented on Fig. 8 indicate that most locations are characterised by an increased concentration of sea-states with crest height ratios of $\eta_c/\eta_F \approx 1$. This means that the second-order model provides accurate predictions for majority of sea-states in these locations. In fact, the mean crest height ratio is typically 1%–3% larger than the Forristall prediction, once all sea-states at each location are considered. There are two noteworthy exceptions to this observation. First, P15 at a water depth of $d = 45$ m has a mean $\eta_c/\eta_F \approx 1.05$. This is due to the nature of the measurements at this location which were segmental during severe weather conditions. As such, the mean ratio is biased towards typically steeper sea-states. Second, P21 at a water depth of $d = 7.7$ m has a mean $\eta_c/\eta_F \approx 0.85$. Given the reduced water depth at this location, this result indicates that the majority of the sea-states are dominated by wave breaking, as described in relation to Fig. 6.

While measured crest heights with $Q = 10^{-3}$ are on average only a few percent larger than second-order predictions, there is considerable scatter in the observed η_c/η_F ratios. With the exception of the shallowest location, these typically vary between 0.95–1.15. This range appears to be consistent across locations indicating that it does not relate to localised effects at a particular platform. Sea-states characterised by amplifications above second-order theory are more common than those exhibiting reductions. More importantly, the observed amplifications typically exceed the inherent statistical variability; the latter being of order 7% for the shortest data bins. In combining these results with the findings of Fig. 6, it is also evident that these amplifications occur during severe incident conditions rather than more benign of average sea-states. At the shallowest location, measured crest heights are significantly lower than predictions across the vast majority of sea-state conditions. This further demonstrates the need to account for wave energy dissipation within the crest height distribution.

4.2. New model formulation

Building upon the experimental and field data findings discussed in Section 4.1, a new crest height model is developed. This model aims to:

1. be applicable across a wide range of effective water depths extending from relatively shallow ($k_p d \approx 0.5$) to deep ($k_p d > 3$) conditions;
2. capture the amplifications beyond the second-order of wave steepness that have been observed in steep sea-states in both field and experimental measurements; and
3. incorporate the effects of wave breaking, limiting the largest crest heights.

To achieve this, the new model has been formulated using the latest understanding of the physical processes that contribute to the formation of the largest crest heights. Any empirical coefficients included in the model have been calibrated using data from two experimental campaigns and a small subset of field measurements. Specifically, experimental data from Test A (Table 1) with $\sigma_\theta = 15°$ and Test B (Table 2) with $\sigma_\theta = 10°$ were employed to cover deep and intermediate water depth conditions. In addition, four storm events recorded at P21 ($d = 7.7$ m) were used to cover the absence of experimental data for $k_p d < 1$. The remaining data were used in the validation of the model in Section 5.

The proposed model is formulated by incrementally including the relevant physical processes that define the largest crest heights. As such, the development of the model begins with the most fundamental assumption of linear wave theory, with additional terms progressively added to represent nonlinear contributions and wave breaking. In adopting this approach, the validity of the model can be assessed at each step and further parametrisations can easily be achieved. The proposed model has the following form:

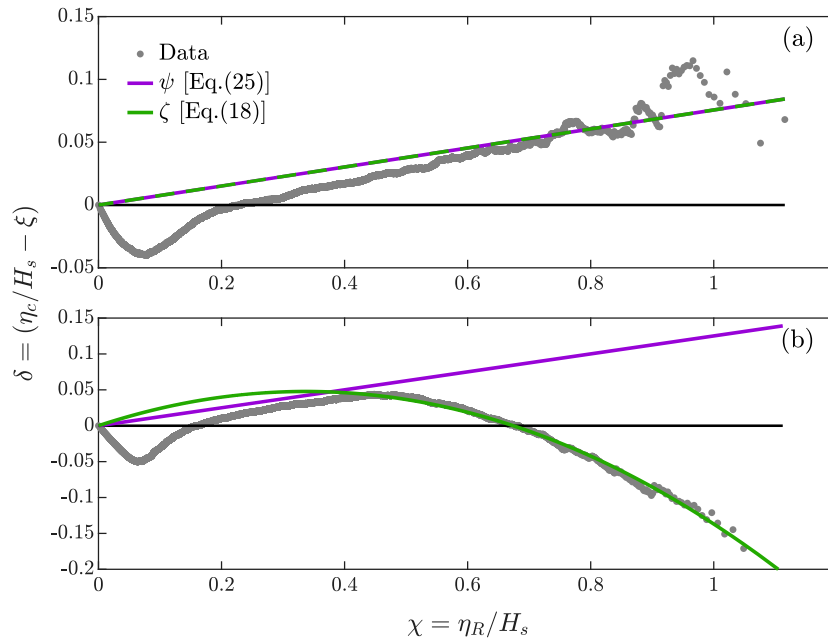$$\eta_M = \left(\eta^{(1)} + \eta^{(2)} + \eta^{(NL)} \right) \cdot f_{Br}, \tag{17}$$

Fig. 9. Examples of the model calibration approach. The difference between measured data and second-order predictions, δ, is plotted against the Rayleigh variate, χ, and compared with the predictions of the nonlinear model, ψ, and final proposed model, ζ. Subplot (a) corresponds to a steep sea-state with little/no wave breaking (case BA4), while subplot (b) corresponds to a sea-state with extensive wave breaking (case BA7).

where η_M represents the crest heights predicted by the new model, $\eta^{(1)}$ is the linear contribution, $\eta^{(2)}$ is the second-order contribution and $\eta^{(NL)}$ is the higher-order nonlinear contribution. Including all effects above second-order. The additional scaling term f_{Br} incorporates the effects of wave breaking. Eq. (17) is best expressed in its non-dimensional form as:

$$\zeta = \frac{\eta_M}{H_s} = \left(\chi + 2\mu\chi^2 + \kappa\mu\chi\right) \cdot (A\chi + B),\qquad(18)$$

where model predictions and individual contributions have been normalised by the significant wave height, H_s. As such, χ represents the fundamental variate used throughout the model and corresponds to the (normalised) Rayleigh-predicted crest heights, $\eta^{(1)}$, as

$$\chi = \frac{\eta^{(1)}}{H_s}.\qquad(19)$$

In terms of completeness, the inverse of the Rayleigh distribution that defines $\eta^{(1)}$ is given by:

$$\eta^{(1)} = \frac{1}{\sqrt{8}} H_s \left(-\ln Q\right)^{1/2},\qquad(20)$$

where Q is the exceedance probability. The remaining terms in Eq. (18) are defined in the paragraphs that follow.

Effects arising at a first-order of wave steepness (linear effects) are well-described by the Rayleigh distribution and are consequently captured through the Rayleigh variate, χ. While the Forristall (2000) distribution provides a good representation of second-order crest heights, an analytically more tractable solution was sought. This is provided by Tayfun (1994) which describes the normalised second-order surface elevation, $\hat{\eta}(t) = \eta(t)/H_s$, as:

$$\hat{\eta}(t) = \chi \cos\phi + 2\mu\chi^2 \cos(2\phi),\qquad(21)$$

where the wave phase function, $\phi(t)$, is uniformly distributed in $[0, 2\pi)$. Upon substituting the trigonometric functions with their expectation, the second-order contribution to the crest heights can be obtained as the second term in Eq. (18). As such, the normalised crest heights, ξ, correct to second-order of wave steepness, are described by:

$$\xi = \frac{\eta^{(1)} + \eta^{(2)}}{H_s} = \chi + 2\mu\chi^2.\qquad(22)$$

This is the inverse of the probability distribution in Eq. (4). In applying this solution, the selection of the steepness parameter, μ, becomes important. Following the work of Tayfun (2006), this is calculated as:

$$\mu = 16\frac{\alpha^3}{\beta}\Gamma\left(\frac{3}{\beta}\right) - \frac{1}{4}\sqrt{\frac{\pi}{2}}\qquad(23)$$

where Γ is the complete gamma function and α and β are the coefficients of the Forristall model given in Eq. (7). This representation of μ incorporates the effects of both sea-state steepness and water depth through S_1 and Ur which define the Forristall coefficients. More importantly, the proposed parametrisation exactly reproduces the predictions of the Forristall (2000) model as shown by Tayfun (2006). Independent numerical simulations, using second-order random wave theory (Sharma and Dean, 1981), undertaken by the authors have verified that the model described in Eqs. (22)–(23) provides an accurate representation of second-order crest height statistics across the full range of water depths investigated herein.

The third term in Eq. (18) describes nonlinear effects arising above second-order. Although the form of this term is, perhaps, not what was initially envisaged, it provides the best description of the higher-order ($> a^2k^2$) nonlinear effects in the measured data; the latter found to scale linearly with χ with a slope of μ. The term κ represents a sigmoid function that acts to introduce these nonlinear effects for steep sea-states. It is defined by:

$$\kappa = \frac{1}{1 + k^3 \exp(-10k\mu)}\qquad(24)$$

with $k = 25.3$. The proposed parametrisation has been obtained through fitting the model of nonlinear crest heights:

$$\psi = \frac{\eta^{(1)} + \eta^{(2)} + \eta^{(NL)}}{H_s} = \chi + 2\mu\chi^2 + \kappa\mu\chi\qquad(25)$$

to experimental data of steep but not breaking sea-states.

Finally, the effects of wave breaking are introduced through the parametrisation of the breaking function, $f_{Br} = A\chi + B$, as:

$$A = \begin{cases} -8.46S_1 + 0.9239Ur^2 - 1.742Ur + 0.5148 & \text{for } \mu > 0.065 \\ 0 & \text{otherwise} \end{cases}\qquad(26)$$
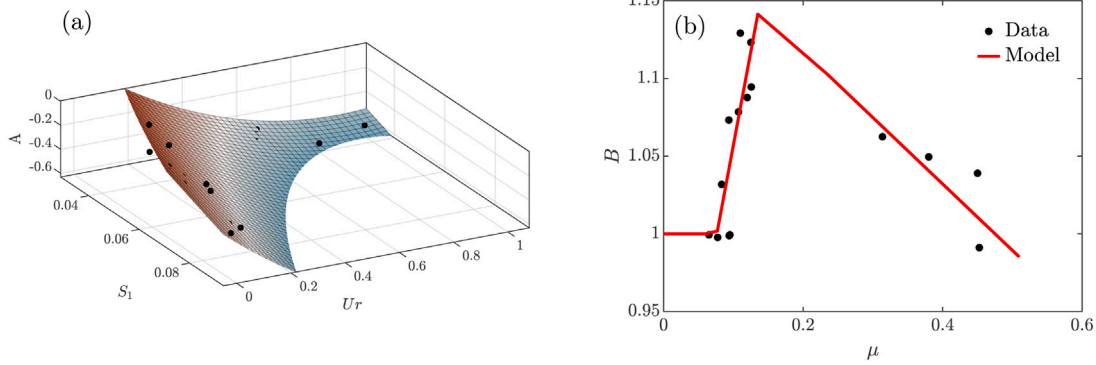
Fig. 10. Coefficients of the breaking parametrisation in the present model. Subplot (a) describes parameter A in Eq. (26), and subplot (b) describes parameter B in Eq. (27). The calibration data points have been added as black bullets for reference.
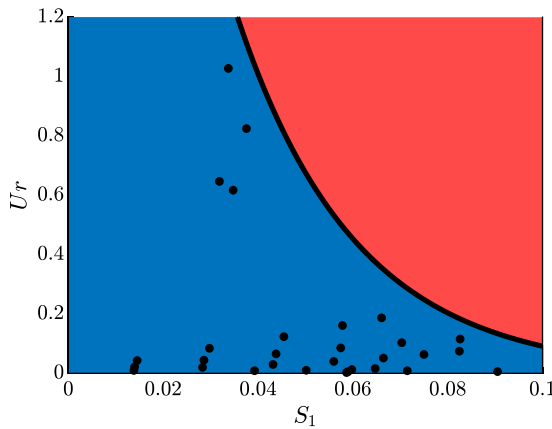

Fig. 11. Validity region of the proposed model (blue) expressed in the (S_1, Ur) parameter space. The test cases used in the calibration of the model are noted as black bullets and Eq. (29) is indicated by the black line. Sea-states in the red region fall outside the model's range of validity. (For interpretation of the references to colour in this figure legend, the reader is referred to the web version of this article.)

and

$$B = \begin{cases} -0.4273\mu + 1.203 & \text{for } \mu \geq 0.16 \\ 2.407\mu + 0.8164 & \text{for } 0.065 < \mu < 0.16 \\ 1 & \text{otherwise.} \end{cases} \tag{27}$$

In practice, the breaking function acts to reduce the crest heights within sea-states that are characterised by extensive wave breaking. This is implemented through the split format of the parametrisation which renders the breaking function inactive for non-breaking sea-states.

The coefficients provided in Eqs. (24)–(27) have been obtained by explicitly modelling the effects of nonlinearity and wave breaking observed in the calibration dataset. This was achieved by first removing linear and second-order effects from the measured crest heights and, subsequently, fitting the differences. Considering that effects up to second-order are well captured by ξ in Eq. (22), these differences were defined by:

$$\delta = \frac{\eta_c}{H_s} - \xi. \tag{28}$$

The subset of sea-states that did not exhibit wave breaking were used to derive ψ in Eq. (25), while those that were breaking to derive f_{Br} and, hence, the final model, ζ, in Eq. (18). To identify those sea-states that are characterised by extensive wave breaking the method described by Karmpadakis and Swan (2020) was employed. In practice, the measured crest heights were compared to numerical simulations correct to a second-order of wave steepness, calculated using the same

input spectra and measuring location. Those sea-states in which the majority of the largest crests fall below the second-order predictions were classified as 'breaking' seas. This classification was then verified by examining the shape of the probability distribution. As discussed in Section 3, sea-states with extensive wave breaking display a characteristic drop in the tail of the crest height distribution and an increase in the crest heights at large exceedance probabilities. Finally, the identification of breaking sea-states was further verified by video recordings taken during the experiment.

Examples of the fitting approach are shown on Fig. 9. The measured differences in the crest height, δ, are expressed as a function of the Rayleigh variate χ for (a) a steep but not breaking sea-state (case BA4), and (b) a very steep sea-state with extensive wave breaking (case BA7). In both cases the effective water depth is $k_p d = 1.53$. The results in Fig. 9(a) suggest that the contributions above second-order are positive and progressively increasing with χ. The parametrisation for ψ is shown to capture this behaviour; the fitting biased towards the largest crest heights since these are most important in a design context. At the same time, the full model, ζ, produces identical results to the nonlinear part, ξ, since there is no (or very limited) wave breaking in this sea-state.

In contrast, Fig. 9(b) shows that the difference δ initially exhibits positive values (larger than second-order) for smaller waves, and then progressively reduces to large negative values (smaller than second-order) for the largest crest heights. In this case, the nonlinear model ψ shows the crest height predictions if wave breaking is completely ignored. This produces a significant over-prediction of the largest crest heights. In contrast, when wave breaking is taken into account, it can be seen that the full model, ζ, can accurately describe the measured crest heights, particularly for $\chi > 0.4$.

It is worth noting that in both cases presented in Fig. 9, there is a region of small crest heights, for $\chi < 0.2$, in which the measured crest heights fall below second-order predictions. This indicates that a smaller second peak is present in the range of very small waves, as has also been observed by Tayfun (2006); the observation being attributed to spectral bandwidth effects. The presence of this secondary peak has no observable effect in the overall distribution of crest heights and, hence, no effort was made to include it in the present model.

The coefficients defining the breaking model parameters, A and B, in Eqs. (26) and (27) were obtained though nonlinear least squares fitting of the breaking sea-states within the calibration dataset. The adjusted R^2 value for parameter A was 97% while for parameter B 90%. Fig. 10 shows the equations derived for parameters A and B alongside the calibration data points. Moreover, Fig. 11 shows the validity range of the present model in the (S_1, Ur) parameter space alongside the sea-states used in its calibration. This parameter space is defined by:
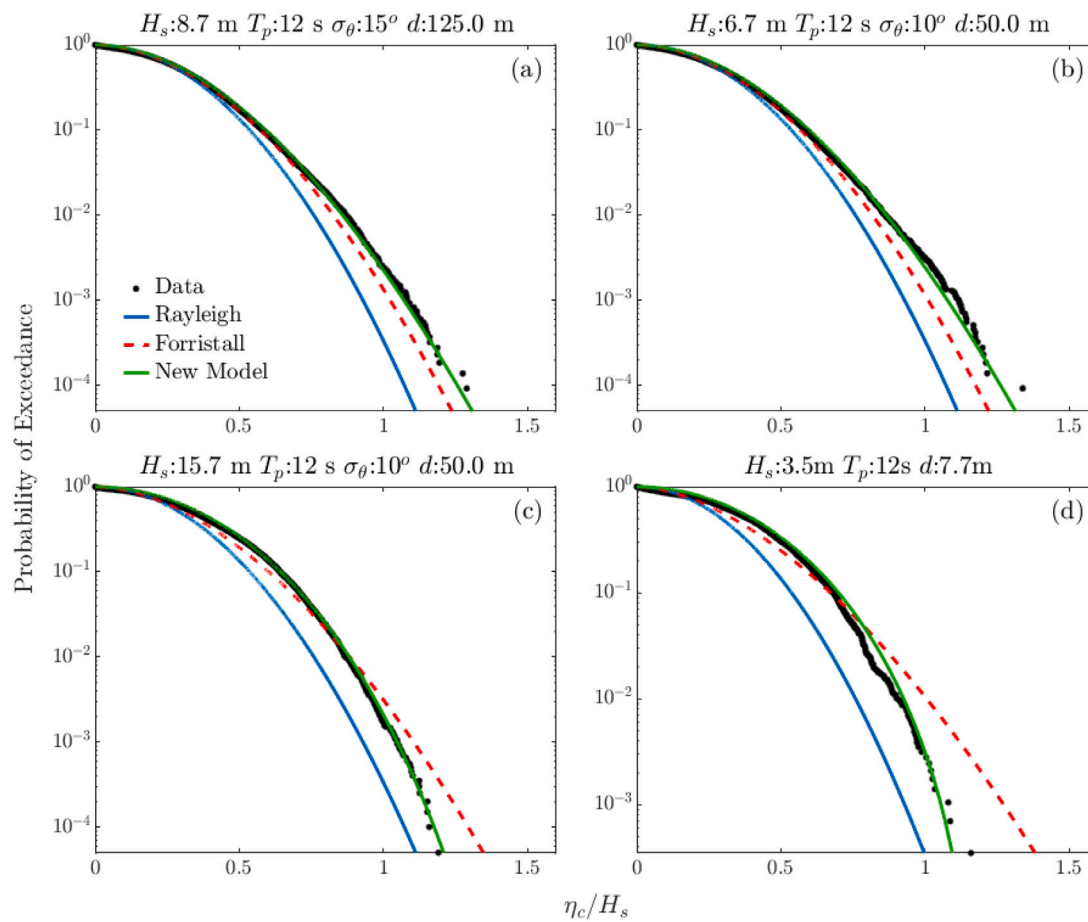
$$Ur < 5 \exp(-45 S_1), \tag{29}$$

Fig. 12. Normalised crest height distributions, η_c/H_s, showing comparisons to linear (Rayleigh), second-order (Forristall) and proposed model predictions. The subplots relate to cases: (a) AA1, (b) BA3, (c) BA7 from the experimental dataset used for the model calibration. Subplot (d) relates to a storm with $H_s = 3.5$ m and $T_p = 12$ s recorded at the field measuring location P21 ($d = 7.7$ m).

and is based on the met–ocean characteristics of the available test cases. It can be seen that there is a significant number of sea-state conditions with $Ur < 0.2$. Importantly, these correspond to a wide range of sea-state steepnesses, S_1. This has allowed the progressive modelling of nonlinear and wave breaking. At the same time, there is a lack of experimental data for $Ur > 0.2$, and measurements from field station P21 have been used to describe the largest $Ur > 0.5$ values. Although unwanted, this lack of experimental measurements on flat bed bathymetries for large Ur numbers is representative of wavemaking limitations in laboratory facilities. In other words, the accurate generation of very steep and shallow water sea-states is a challenging task. While the introduction of a bed slope can provide the required shallow water conditions, its effects need to be carefully considered (Karmpadakis et al., 2022).

Evidence of the success of the new model is provided in Fig. 12. Each plot compares the distribution of measured crest heights with the predictions of the new model, the Forristall and Rayleigh distributions. All the sea-states considered belong to the calibration dataset and have been selected to represent the widest range of effective water depths. Fig. 12(a) relates to the deep water case AA1 with effective water depth $k_p d = 3.5$ and sea-state steepness $S_p \approx 0.04$. The observed amplifications above the Forristall model for $Q < 10^{-2}$ are well described by the proposed model. Fig. 12(b) shows that the new model is equally successful in the intermediate water depth case BA3 with $k_p d = 1.53$ and $S_p = 0.03$. In both cases, the key feature of the sea-states is the increase of the measured crest heights above the second-order model.

Considering sea-states that are characterised by extensive wave breaking, Fig. 12(c) concerns the intermediate water depth case BA7,

with $k_p d = 1.53$ and $S_p = 0.07$. In this case, the observed reduction in the tail of the distribution compared to second-order predictions is well described by the new model. Finally, Fig. 12(d) presents results arising in a single storm event recorded at the shallowest measuring location in the field (P21). The data correspond to a sea-state with $k_p d = 0.5$ and $S_p = 0.015$. Considering the shallow depth and the severity of this case, it is clear that wave breaking plays a significant role. This becomes apparent by noting the large reductions in crest heights for $Q < 10^{-1}$ when compared to second-order predictions. More importantly, it is clear that the new model is successful in capturing this behaviour.

5. Model validation

While the development of a successful model to describe such a wide range of water depths and steepnesses is a challenge in its own right, it is also important to demonstrate the success of the model in respect of data, particularly field data, that was not used in the model calibration and to explore its success in respect of conditions that lie outside the range of the calibration data. In the figures that follow, the individual crest heights, η_c, have been normalised by the significant wave height, H_s, and plotted against their exceedance probability, Q. In all cases, the measured data are compared to the predictions of the Rayleigh and Forristall distributions, as well as the proposed model.

Fig. 13 provides a selection of cases from the 4 experimental datasets. The sea-states considered cover the full range of water depths available in the experimental investigation ($d = 125$ m, 90 m, 50 m and 45 m), various directional spreads in the range $\sigma_\theta = 20° - 33°$ and a broad range of sea-state steepnesses. These cases have been selected to

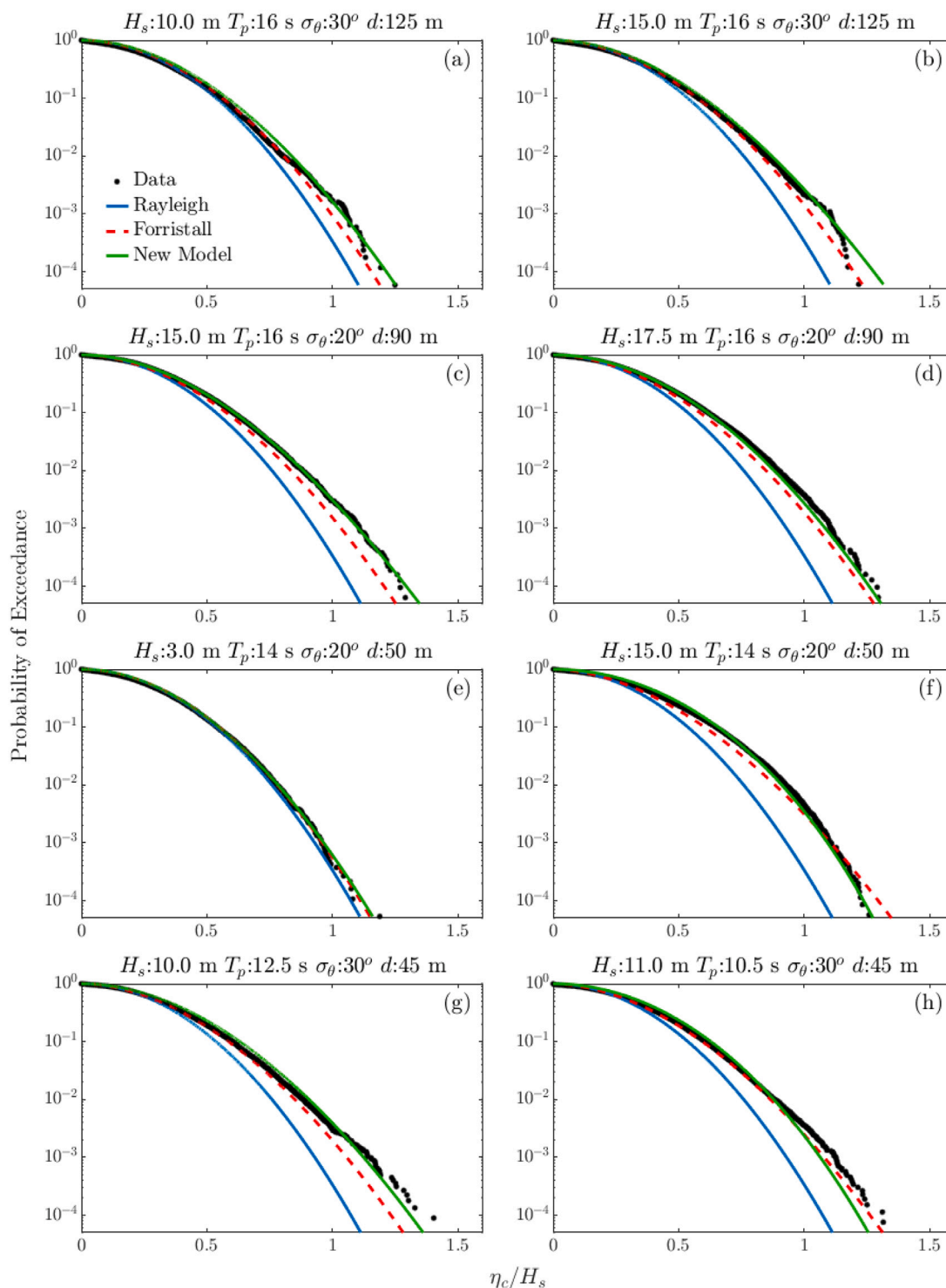**Fig. 13.** Normalised crest height distributions, η_c/H_s, recorded in different experimental facilities and showing comparisons to linear (Rayleigh), second-order (Forristall) and proposed model predictions. The subplots relate to cases: (a) AC2, (b) AC4, (c) C5, (d) C6, (e) BB1, (f) BB5, (g) DB2 and (h) DA1.

include two sea-states in each water depth and to provide evidence of the model performance for mild, steep and very steep sea-states. Specifically, Figs. 13(a)–(b) relate to measurements in $d = 125\,\text{m}$, with $T_p = 16\,\text{s}$ and $\sigma_\theta = 30°$. The significant wave heights are $H_s = 10\,\text{m}$ and 15 m, respectively. In both cases the measured crest heights exhibit nonlinear amplifications above the Rayleigh and Forristall models. The new model is shown to be in good agreement with the measurements. Data relating to $d = 90\,\text{m}$ is presented in subplots (c) and (d). These sea-states are characterised by $T_p = 16\,\text{s}$, $\sigma_\theta = 20°$ and $H_s = 15\,\text{m}$ and

17.5 m, respectively. Once again, the linear and second-order models under-predict large crest heights. While the measured crest heights in Fig. 13(d) remain above the Forristall predictions, some wave breaking was observed. In both these cases, the new model is again shown to provide a better representation of the measured data, although it marginally under-predicts the largest crest heights in the steeper case (Fig. 13(d)).

Figs. 13(e)–(f) relate to sea-states in $d = 50\,\text{m}$, with $T_p = 14\,\text{s}$ and $\sigma_\theta = 20°$. Subplot (e) corresponds to a very mild sea-state with
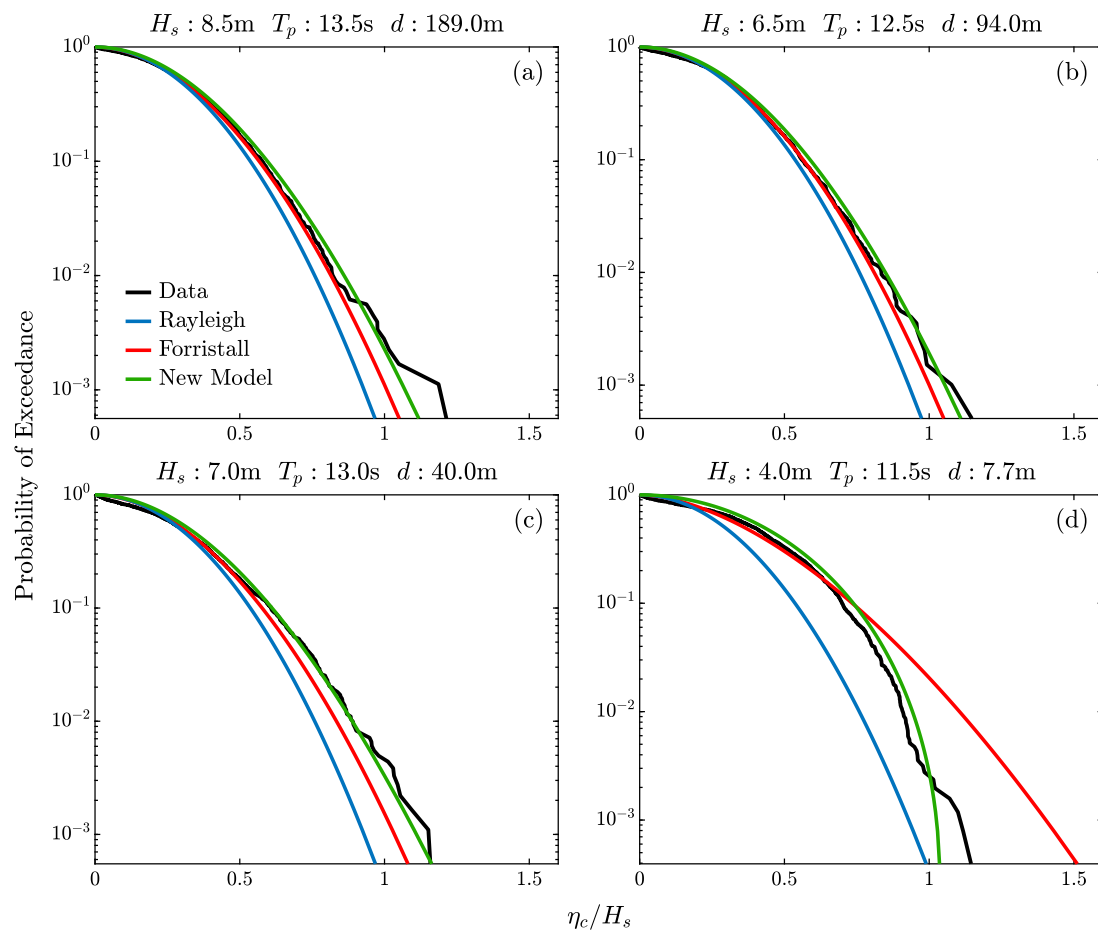
Fig. 14. Normalised crest height distributions, η_c/H_s, recorded in the field and showing comparisons to linear (Rayleigh), second-order (Forristall) and proposed model predictions. The subplots represent selected data bins within locations: (a) P1, (b) P9, (c) P13 and (d) P21, in accordance with the contour plots of Fig. 7. Water depth and sea-state information are included in the subplot titles.

$H_s = 3$ m. In this case the measured crest heights are marginally larger than the Rayleigh model and well described by the Forristall model. Importantly, the new model approximates the second-order solution and fits the data well. This demonstrates the capability of the model to describe less severe sea-states in which higher order nonlinearities and wave breaking are of reduced importance. Subplot (f) corresponds to a steep sea-state characterised by a considerable degree of wave breaking. The measured crest heights are now lower than the second-order model in the tail of the distribution and larger for smaller waves with $Q \approx 10^{-2}$. The observed shape of the distribution is characteristic of breaking sea-states in which the largest crest heights experience energy dissipation which is redistributed towards smaller waves. The proposed model is shown to capture this behaviour both qualitatively and quantitatively. Similar results are obtained in Figs. 13(g)–(h) for a water depth of $d = 45$ m and a directional spread of $\sigma_\theta = 33°$. Subplot (g) relates to a sea-state with $H_s = 10$ m and $T_p = 12.5$ s, while subplot (h) to a steeper sea-state with $H_s = 11$ m and $T_p = 10.5$ s. In both cases, the proposed model is shown to be in good agreement with the data, although some deviations at the tail of the distribution can be observed particularly in the last case.

At this point, it is worth noting that the present model has been calibrated on the basis of sea-states with directional spreads of $\sigma_\theta = 10° - 15°$. As such, the effects of increased short-crestedness have not been explicitly incorporated. In this respect the minor discrepancies recorded above could be attributed to the directional effects described by Latheef and Swan (2013) and Karmpadakis et al. (2019). However, such effects (involving subtle changes in the directional spread) are shown to have a relatively small impact on the overall crest height

distribution and are confined to differences of the order of 2%–3% with respect to model predictions. However, further investigation including sea-states with broader directional spreads is required to obtain a robust parametrisation of the effects of directionality. Fortunately, the modular form of the present model allows for such amendments with relative ease.

The final step towards an effective validation of the proposed model involves comparisons to representative field data. Adopting a similar representation to the experimental results, data recorded at 4 measuring locations with $d = 189$ m, 94 m, 40 m and 7.7 m are compared to model predictions in Fig. 14. The sea-states included within this Figure are characterised by the largest errors with respect to the Forristall model at each location, as identified in Fig. 6 and presented in Fig. 7. In this respect they correspond to the most severe sea-states at each location. In comparing the measured data to model predictions, it is clear that the proposed model provides the best fit in this very wide range of severe conditions. These include cases in which clear amplifications above the Forristall model are observed (subplots (a) and (c)); cases in which small discrepancies with respect to the Forristall model are observed (subplot (b)); and cases in which the effects of wave breaking are clearly very important (subplot (d)). Despite small deviations from the proposed model, there is broad agreement in all these cases and a clear improvement over existing models.

6. Conclusions and wider practical (design) implications

The present paper has considered the short-term distribution of crest heights occurring in a very wide range of water depths and sea-states. Having assembled and analysed two extensive data sets, one
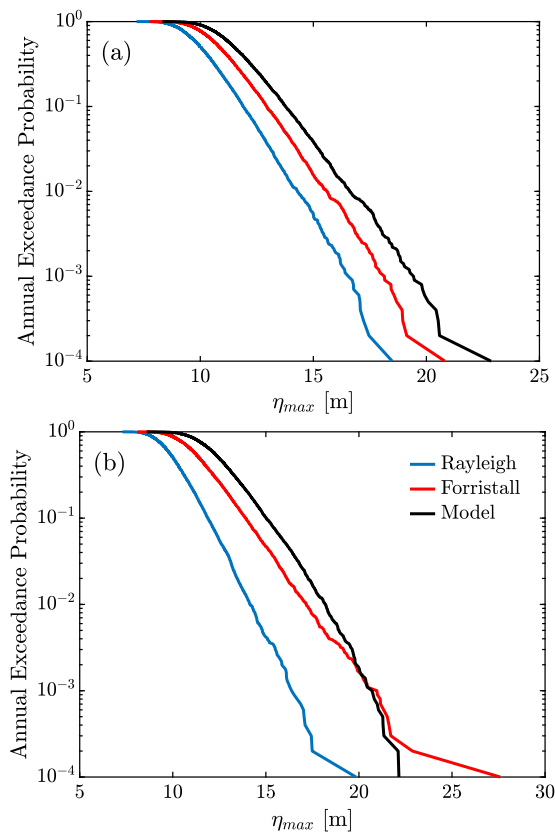
Fig. 15. Long-term distribution of maximum crest height, η_{max} for water depths of (a) $d = 150\,\mathrm{m}$ and (b) $d = 40\,\mathrm{m}$. The annual exceedance probabilities corresponding to the Rayleigh, Forristall and present models are compared.

based on laboratory observations and the second field data, the inappropriateness of defining the largest crest heights in terms of weakly nonlinear, second-order, calculations is clear. The explanation for this lies in two parts: the nonlinear amplification of crest heights due to wave interactions occurring beyond a second-order of wave steepness, and the dissipative effects of wave breaking. The balance between these competing processes determines whether crest heights are increased or reduced relative to second-order predictions; the latter forming the basis of present design practice. Indeed, it is important to note, that both the laboratory and the field data provide numerous examples of both increases and reductions in the crest heights associated with small exceedance probabilities.

Having established these important effects, a new crest height distribution appropriate to a wide range of water depths and sea-states has been proposed. This model builds upon earlier work in terms of its analytic construction and has been calibrated on the basis of experimental data and a small sub-set of field measurements; the latter filling an important gap in the parameter space of the former. Once complete, the model has been validated using independent experimental data from multiple laboratory facilities and a very wide range of field data gathered at 21 North Sea locations.

The new model has been shown to provide considerable improvements over existing models in the vast majority of cases considered. Most importantly, it has been shown to successfully predict the changes in the crest height distribution arising due to the nonlinear amplifications and the dissipative effects of wave breaking. The latter incorporating both steepness-induced wave breaking in deeper water and depth-induced wave breaking in shallower water. Importantly, the proposed model is directly relevant to design calculations, being no more difficult to apply than the existing design standard (Forristall,

2000). Moreover, the model is presented in a modular form in the sense that it parametrically describes individual physical processes separately before bringing everything together. In this respect, each component of the model can be assessed individually and improved (if necessary) as more data become available.

Finally, it is important to place the proposed model in the context of practical design calculations. If, as is often the case, the design philosophy is based upon a simplified quasi-deterministic approach in which the largest wave crest is believed to produce the largest wave load and is assumed to occur in the most severe sea-state defined by the peak of the N-year environmental contour (Ross et al., 2020); where N may be 100 or 10,000 depending on the type of structure or the prevailing design codes. In this case the present model can be applied, in exactly the same way as the Forristall (2000) model, to determine the maximum crest elevation arising in this sea-state. This may be larger or smaller than present design calculations. If it is smaller, then it implies that wave breaking is important and this must be incorporated within the predicted water particle kinematics. This opens the possibility that a smaller, but breaking wave, may generate larger loads. In this sense, the proposed model is not only able to provide a better estimate of the design crest height in a given storm, but also allows inferences to be drawn as to how that wave should be modelled.

Alternatively, if a full probabilistic analysis is required to determine the annual probability of failure, the short–term distribution of wave crests arising in individual storms must be integrated over all possible storms to produce a long-term distribution of crest heights. The statistical basis for such an approach is given by Heffernan and Tawn (2004) with best practice in terms of practical applications outlined by Ross et al. (2020). Whilst the details of the preferred approach lies beyond the scope of the present paper, it is important to note that all approaches required a short–term distribution of crest heights. In present practice this would be provided by Forristall (2000), but this could easily be replaced by the proposed model allowing the incorporation of full (higher-order) nonlinearity and wave breaking. In recommending such an approach, one key question arises: to what extent do the competing influences on nonlinear amplification and the dissipative effects of wave breaking cancel each other out when integrated over all possible storms.

Adopting the recommendations of Ross et al. (2020) and performing full long-term calculations based upon the linear (Rayleigh) model, the second-order Forristall (2000) model and the present model allows the impact of nonlinearity and breaking to be assessed in an engineering design context. The results of such a calculation are given on Fig. 15; subplot (a) addressing deep water conditions and subplot (b) shallower water.

In the deep-water comparisons it is clear that the inclusion of nonlinearity beyond second-order can lead to increases in the long-term distribution of crest heights; the extent of the increase depending on the steepness of the sea-states arising in individual storms. In contrast, in shallower water wave breaking becomes more important and the long-term distributions of crest heights falls below those predicted by the second-order models used in present design practice. The practical implications of these changes are significant. For example, if the failure of a structure is primarily driven by a loss of air-gap and the occurrence of wave-in-deck loading, the new model suggests that present design practice is likely to be conservative in shallow water, but non-conservative in deep water. This is broadly consistent with a recent review by the Health & Safety Executive (HSE, 2018) of the integrity of fixed structures on the UK continental shelf.

CRediT authorship contribution statement

I. Karmpadakis: Conceptualization, Formal analysis, Investigation, Methodology, Visualization, Writing – original draft, Writing – review & editing. **C. Swan:** Conceptualization, Funding acquisition, Writing – review & editing.

Declaration of competing interest

The authors declare that they have no known competing financial interests or personal relationships that could have appeared to influence the work reported in this paper.

Data availability

Data will be made available on request.

Acknowledgements

References

Allender, J., Audunson, T., Barstow, S.F., Bjerken, S., Krogstad, H.E., Steinbakke, P., Vartdal, L., Borgman, L.E., Graham, C., 1989. The wadic project: A comprehensive field evaluation of directional wave instrumentation. Ocean Eng. 16 (5–6), 505–536. http://dx.doi.org/10.1016/0029-8018(89)90050-4.

Andreasen, K.K., Skourup, J., Hansen, N.E.O., Andreasen, K.K., 1997. Non-Gaussian Extreme Waves in the Central North Sea. J. Offshore Mech. Arct. Eng. 119 (3), 146–150. http://dx.doi.org/10.1115/1.2829061.

Bitner, E.M., 1980. Non-linear effects of the statistical model of shallow-water wind waves. Appl. Ocean Res. 2 (2), 63–73. http://dx.doi.org/10.1016/0141-1187(80)90031-0.

Bitner-Gregersen, E.M., Magnusson, A.K., 2004. Extreme events in field data and in a second order wave model. Rogue Waves 1–16.

Buchner, B., Forristall, G., Ewans, K.C., Christou, M., Henning, J., 2011. New insights in extreme crest height distributions (A summary of the CresT JIP). In: Proceedings of 30th International Conference on Offshore Mechanics and Arctic Engineering. pp. 1–16. http://dx.doi.org/10.1115/OMAE2011-49846.

Casas-Prat, M., Holthuijsen, L.H., 2010. Short-term statistics of waves observed in deep water. J. Geophys. Res.: Oceans 115 (9), 1–20. http://dx.doi.org/10.1029/2009JC005742.

Cherneva, Z., Tayfun, M.A., Guedes Soares, C., 2009. Statistics of nonlinear waves generated in an offshore wave basin. J. Geophys. Res. 114 (C8), C08005. http://dx.doi.org/10.1029/2009JC005332.

Christou, M., Ewans, K., 2014. Field Measurements of Rogue Water Waves. J. Phys. Oceanogr. 44 (9), 2317–2335. http://dx.doi.org/10.1175/JPO-D-13-0199.1.

DNV-RP-C205, 2017. Environmental Conditions and Environmental Loads. In: Det Norske Veritas.

Fedele, F., Brennan, J., Ponce De León, S., Dudley, J., Dias, F., 2016. Real world ocean rogue waves explained without the modulational instability. Sci. Rep. 6 (May), 1–11. http://dx.doi.org/10.1038/srep27715.

Fedele, F., Herterich, J., Tayfun, A., Dias, F., 2019. Large nearshore storm waves off the Irish coast. Sci. Rep. 9 (1), 15406. http://dx.doi.org/10.1038/s41598-019-51706-8.

Fedele, F., Tayfun, M.A., 2009. On nonlinear wave groups and crest statistics. J. Fluid Mech. 620, 221–239. http://dx.doi.org/10.1017/S0022112008004424.

Forristall, G.Z., 2000. Wave Crest Distributions: Observations and Second-Order Theory. J. Phys. Oceanogr. 30 (8), 1931–1943. http://dx.doi.org/10.1175/1520-0485(2000)030<1931:WCDOAS>2.0.CO;2.

Gibson, R., Christou, M., Feld, G., 2014. The statistics of wave height and crest elevation during the December 2012 storm in the North Sea. Ocean Dyn. 64 (9), 1305–1317. http://dx.doi.org/10.1007/s10236-014-0750-5.

Hasselmann, K., Barnett, T.P., Bouws, E., Carlson, H., Cartwright, D.E., Enke, K., Ewing, J.A., Gienapp, H., Hasselmann, D.E., Kruseman, P., Meerburg, A., Muller, P., Olbers, D.J., Richter, K., Sell, W., Walden, H., 1973. Measurements of Wind-Wave Growth and Swell Decay during the Joint North Sea Wave Project (JONSWAP). Ergnzungsheft Dtsch. Hydrogr. Z. Reihe A(8) (12), p.95.

Heffernan, J.E., Tawn, J.A., 2004. A conditional approach for multivariate extreme values. J. R. Stat. Soc. Ser. B Stat. Methodol. 66 (3), 497–546. http://dx.doi.org/10.1111/j.1467-9868.2004.02050.x.

Herbers, T.H., Janssen, T.T., 2016. Lagrangian surface wave motion and Stokes drift fluctuations. J. Phys. Oceanogr. 46 (4), 1009–1021. http://dx.doi.org/10.1175/JPO-D-15-0129.1.

Holthuijsen, L.H., 2007. Waves in Oceanic and Coastal Waters. vol. 9780521860, Cambridge University Press, pp. 1–387. http://dx.doi.org/10.1017/CBO9780511618536.

HSE, 2018. Extreme environmental loading of fixed offshore structures. URL: https://www.hse.gov.uk/offshore/research/extreme-wave.htm.

ISO 19901-1, 2015. Petroleum and natural gas industries — Specific requirements for offshore structures — Part 1: Metocean design and operating considerations.

James, I.D., 1986. A note on the theoretical comparison of wave staffs and wave rider buoys in steep gravity waves. Ocean Eng. 13 (2), 209–214. http://dx.doi.org/10.1016/0029-8018(86)90028-4.

Karmpadakis, I., 2018. Wave Statistics in Intermediate and Shallow Water Depths (Ph.D. thesis). Imperial College London.

Karmpadakis, I., Swan, C., 2020. On the Average Shape of the Largest Waves in Finite Water Depths. J. Phys. Oceanogr. 50 (4), 1023–1043. http://dx.doi.org/10.1175/JPO-D-19-0165.1.

Karmpadakis, I., Swan, C., Christou, M., 2019. Laboratory investigation of crest height statistics in intermediate water depths. Proc. R. Soc. A 475 (2229), 20190183. http://dx.doi.org/10.1098/rspa.2019.0183.

Karmpadakis, I., Swan, C., Christou, M., 2020. Assessment of wave height distributions using an extensive field database. Coast. Eng. 157, 103630. http://dx.doi.org/10.1016/j.coastaleng.2019.103630.

Karmpadakis, I., Swan, C., Christou, M., 2022. A new wave height distribution for intermediate and shallow water depths. Coast. Eng. 175, 104130. http://dx.doi.org/10.1016/j.coastaleng.2022.104130.

Katsardi, V., de Lutio, L., Swan, C., 2013. An experimental study of large waves in intermediate and shallow water depths. Part I: Wave height and crest height statistics. Coast. Eng. 73, 43–57. http://dx.doi.org/10.1016/j.coastaleng.2012.09.007.

Katsardi, V., Swan, C., 2011. The evolution of large non-breaking waves in intermediate and shallow water. I. Numerical calculations of uni-directional seas. Proc. R. Soc. A 467 (2127), 778–805. http://dx.doi.org/10.1098/rspa.2010.0280.

Latheef, M., Swan, C., 2013. A laboratory study of wave crest statistics and the role of directional spreading. Proc. R. Soc. A 469 (2152), http://dx.doi.org/10.1098/rspa.2012.0696, 20120696.

Latheef, M., Swan, C., Spinneken, J., 2017. A laboratory study of nonlinear changes in the directionality of extreme seas. Proc. R. Soc. A http://dx.doi.org/10.1098/rspa.2016.0290.

Longuet-Higgins, M.S., 1952. On the statistical distribution of the heights of sea waves. J. Mar. Res. 11 (3), 245–266.

Longuet-Higgins, M.S., 1963. The effect of non-linearities on statistical distributions in the theory of sea waves. J. Fluid Mech. 17 (03), 459. http://dx.doi.org/10.1017/S0022112063001452.

Ma, L., Swan, C., 2020. The effective prediction of wave-in-deck loads. J. Fluids Struct. 95, 102987. http://dx.doi.org/10.1016/j.jfluidstructs.2020.102987.

Magnusson, A.K., Donelan, M.A., Drennan, W.M., 1999. On estimating extremes in an evolving wave field. Coast. Eng. 36 (2), 147–163. http://dx.doi.org/10.1016/S0378-3839(99)00004-6.

Masterton, S.R., Swan, C., 2008. On the accurate and efficient calibration of a 3D wave basin. Ocean Eng. 35, 763–773. http://dx.doi.org/10.1016/j.oceaneng.2008.02.002.

McAllister, M.L., van den Bremer, T.S., 2019. Lagrangian measurement of steep directionally spread ocean waves: Second-order motion of a wave-following measurement buoy. J. Phys. Oceanogr. 49 (10), http://dx.doi.org/10.1175/JPO-D-19-0170.1.

Mitsuyasu, H., Tasai, F., Suhara, T., Mizuno, S., Ohkusu, M., Honda, T., Rikiishi, K., 1975. Observations of the Directional Spectrum of Ocean WavesUsing a Cloverleaf Buoy. J. Phys. Oceanogr. 5 (4), 750–760. http://dx.doi.org/10.1175/1520-0485(1975)005<0750:OOTDSO>2.0.CO;2.

Onorato, M., Waseda, T., Toffoli, A., Cavaleri, L., Gramstad, O., Janssen, P.A., Kinoshita, T., Monbaliu, J., Mori, N., Osborne, A.R., Serio, M., Stansberg, C.T., Tamura, H., Trulsen, K., 2009. Statistical properties of directional ocean waves: The role of the modulational instability in the formation of extreme events. Phys. Rev. Lett. 102 (11), 18–21. http://dx.doi.org/10.1103/PhysRevLett.102.114502.

Petrova, P., Cherneva, Z., Guedes Soares, C., 2006. Distribution of crest heights in sea states with abnormal waves. Appl. Ocean Res. 28 (4), 235–245. http://dx.doi.org/10.1016/j.apor.2007.01.001.

Rademakers, P., 1993. Waverider-wavestaff comparison. Ocean Eng. 20 (2), 187–193. http://dx.doi.org/10.1016/0029-8018(93)90034-F.

Ross, E., Astrup, O.C., Bitner-Gregersen, E., Bunn, N., Feld, G., Gouldby, B., Huseby, A., Liu, Y., Randell, D., Vanem, E., Jonathan, P., 2020. On environmental contours for marine and coastal design. Ocean Eng. 195 (June 2019), 106194. http://dx.doi.org/10.1016/j.oceaneng.2019.106194.

Schubert, M., Wu, Y., Tychsen, J., Dixen, M., Faber, M.H., Sørensen, J.D., Jonathan, P., 2020. On the distribution of maximum crest and wave height at intermediate water depths. Ocean Eng. 217 (May), http://dx.doi.org/10.1016/j.oceaneng.2020.107485.

Sharma, J., Dean, R., 1981. Second-Order Directional Seas and Associated Wave Forces. Soc. Petrol. Eng. J. 21 (01), 129–140. http://dx.doi.org/10.2118/8584-PA.

Socquet-Juglard, H., Dysthe, K., Trulsen, K., Krogstad, H.E., Liu, J., 2005. Probability distributions of surface gravity waves during spectral changes. J. Fluid Mech. 542 (2005), 195–216. http://dx.doi.org/10.1017/S0022112005006312.

Spinneken, J., Swan, C., 2012. The operation of a 3D wave basin in force control. Ocean Eng. 55, 88–100. http://dx.doi.org/10.1016/j.oceaneng.2012.07.024.

Stansell, P., Wolfram, J., Linfoot, B., 2002. Effect of sampling rate on wave height statistics. Ocean Eng. 29 (9), 1023–1047. http://dx.doi.org/10.1016/S0029-8018(01)00066-X.

Tayfun, M.A., 1980. Narrow-band nonlinear sea waves. J. Geophys. Res. 85 (C3), 1548. http://dx.doi.org/10.1029/JC085iC03p01548.

Tayfun, M.A., 1993. Sampling-Rate Errors in Statistics of Wave Heights and Periods. J. Waterway Port Coast. Ocean Eng. 119 (2), 172–192. http://dx.doi.org/10.1061/(ASCE)0733-950X(1993)119:2(172).

Tayfun, M.A., 1994. Distributions of Envelope and Phase in Wind Waves. J. Phys. Oceanogr. 38 (12), 2784–2800. http://dx.doi.org/10.1175/2008JPO4008.1.

Tayfun, M.A., 2006. Statistics of nonlinear wave crests and groups. Ocean Eng. 33 (11–12), 1589–1622. http://dx.doi.org/10.1016/j.oceaneng.2005.10.007.

Tayfun, M.A., Fedele, F., 2007. Wave-height distributions and nonlinear effects. Ocean Eng. 34 (11–12), 1631–1649. http://dx.doi.org/10.1016/j.oceaneng.2006.11.006.

Tayfun, M.A., Lo, J., 1990. Nonlinear Effects on Wave Envelope and Phase. J. Waterw. Port Coast. Ocean Eng. 116 (1), 79–100. http://dx.doi.org/10.1061/(ASCE)0733-950X(1990)116:1(79).

Xiao, W., Liu, Y., Wu, G., Yue, D.K.P., 2013. Rogue wave occurrence and dynamics by direct simulations of nonlinear wave-field evolution. J. Fluid Mech. 720, 357–392. http://dx.doi.org/10.1017/jfm.2013.37.

Zve, E., 2022. Nonlinear Wave Interactions and Crest Height Predictions for Sea-States in Finite Water Depth (Ph.D. thesis). Imperial College London.